Deep electronic gap levels induced by isovalent P and As impurities in GaN

T. Mattila[1] and Alex Zunger[2]
National Renewable Energy Laboratory, Golden, Colorado 80401

The electronic and atomic structure of isovalent substitutional P and As impurities in GaN is studied theoretically using self-consistent plane-wave pseudopotential method. In contrast with all conventional isovalent III-V systems, Ga<u>N</u>:P and Ga<u>N</u>:As are shown to exhibit *deep* gap levels. The calculated donor energies are $\epsilon(+/0) = \epsilon_v + 0.22$ and $\epsilon_v + 0.41$ eV, respectively, and the double donor energies are $\epsilon(++/+) = \epsilon_v + 0.09$ and $\epsilon_v + 0.24$ eV, respectively. The p-like gap wavefunction is found to be strongly localized on the impurity site. Outward atomic relaxations of $\sim 13\%$ and $\sim 15\%$ are detected for the nearest neighbor Ga-atoms surrounding neutral Ga<u>N</u>:P^0 and Ga<u>N</u>:As^0, respectively. The relaxation increases by $\sim 1\%$ for the positively charged impurities. The impurity-bound exciton binding energy is calculated at $E_b = 0.22$ and $E_b = 0.41$ eV for Ga<u>N</u>:P and Ga<u>N</u>:As. The former is in good agreement with the experimental data ($E_b = 0.232$ eV) whereas the latter is offered as a prediction. No clear Jahn-Teller symmetry lowering ($T_d \rightarrow C_{3v}$) distortion, suggested by the one-electron configuration, is found for Ga<u>N</u>:P^+ and Ga<u>N</u>:As^+.

I. INTRODUCTION

In most semiconductors, *isovalent* impurities do not induce defect energy levels in the band gap. For example, substitution of Si in Ge or Ge in Si, or any cross substitution between AlX/GaX/InX (where X=P, As, Sb), does not produce deep gap levels. Instead, the band edges are displaced as a whole as the composition of an isovalent impurity species is increased [1]. Recently, however, an exception to this rule was predicted for III-V compounds: It was shown, via pseudopotential calculations [2–4], that substitutional P and As in GaN (denoted Ga<u>N</u>:P and Ga<u>N</u>:As, respectively) have *deep* single-particle energy levels at $\epsilon_v + 0.61$ eV and $\epsilon_v + 0.75$ eV, respectively, where ϵ_v denotes the valence band maximum. This behavior is analogous with II-VI compounds where the isovalent impurities Cd<u>S</u>:Te [5–9], and Zn<u>S</u>:Te [10,11,7] are known to induce *deep* gap states.

The origin of the deep gap levels is the considerable mismatch in size and orbital energies between the substituted isovalent species. The size mismatch leads to large lattice relaxation and consequently to the localization of the electronic wavefunctions [2–4]. The localization has dramatic effects on the electronic properties of the system as a function of impurity concentration: while in conventional alloys the band gap changes continuously and smoothly as the "impurity" (=alloy) composition x is increased, in the presence of localized isovalent gap states, even small impurity concentrations are capable of inducing radical changes in the size of the effective band gap. At the dilute limit $x \ll 1$, optical transition energies are predicted to be "pinned" at the impurity level inside the band gap (e.g., conduction band-to-impurity transitions). For larger concentrations the impurity level broadens. This was exemplified by the experimental detection of anomalously large ($\sim$ 20 eV) optical bowing coefficients in the case of $GaAs_{1-x}N_x$ alloys [12,13]. Recent theoretical studies have indeed shown that the origin of this behavior is the wavefunction localization at impurity lattice sites, which leads to discontinuities in the band gap behavior in the dilute impurity limit in $GaAs_{1-x}N_x$ [14–16,2–4].

The previous theoretical studies [2–4] used an empirical pseudopotential method (EPM). The purpose of this paper is to study theoretically in more detail the isovalent impurities Ga<u>N</u>:As and Ga<u>N</u>:P, and the associated luminescence transitions observed in Refs. [17–19], using first-principles electronic structure techniques.. The experimental studies [17–19] for P (As) implanted GaN samples revealed PL lines at ~ 2.9 (~ 2.6) eV. In the absence of relaxation, this energy would correspond to the position of the impurity-induced level at $\epsilon_v + 0.6$ ($\epsilon_v + 0.9$) eV above the valence band maximum. However, Jadwisienczak and Lozykowski [19] have determined the zero phonon line to reside at 3.2709 eV in the case of Ga<u>N</u>:P, so the *relaxed* position is at $\epsilon_v + 0.232$ eV, rather than the value $\epsilon_v + 0.6$ eV obtained from PL. In our computational approach we use the self-consistent plane-wave pseudopotential method [20] based on density-functional theory (DFT) [21] in the local-density approximation (LDA) [22,23]. The computational details are described Sec. III A below. Our results can be summarized as follows: (i) the LDA calculations verify the deep character of isolated As and P impurities in GaN leading to the appearance of triply degenerate t_2 levels in the band gap. We find good qualitative agreement in the position of the single-particle impurity levels between empirical and first-principles pseudopotential results. (ii) evaluation of the zero-phonon line and exciton binding energy requires self-consistent total energy and relaxation calculations that are impossible with the empirical pseudopotential method. We use for this purpose the LDA method, and find the exciton binding energy for Ga$\underline{\text{N}}$:P at $E_b = \epsilon_v + 0.22$ eV, in excellent agreement with the recent experimental photoluminescence data ($E_b = \epsilon_v + 0.232$ eV) [19]. (iii) Although the one-electron configuration of the positively charged defects (Ga$\underline{\text{N}}$:P$^+$ and Ga$\underline{\text{N}}$:As$^+$) suggests the possibility of a Jahn-Teller distortion, LDA total energy calculations do not predict that these symmetry lowering relaxations ($T_d \rightarrow C_{3v}$) are energy-lowering.

II. DESCRIPTION OF THE PHOTOLUMINESCENCE PROCESS VIA TOTAL ENERGIES

Our purpose is to calculate the binding energy of the impurity-bound exciton. Given the type of experimental data that are available [17–19], we first discuss the microscopic interpretation of the measured transitions, so as to establish what needs to be calculated. Figure 1 illustrates schematically the states involved in the photoluminescence processes associated with deep centers. We depict total energies as a function of the atomic positions in the system described by a configuration coordinate Q. The lowest state $E[V^nD^mC^0]$ depicts the equilibrium ground state of the neutral defect with fully occupied valence (n electrons) and defect (m electrons) levels and with empty conduction band. Consider now the following five-step process:

(i) upon excitation with above-band-gap energy photons, an electron is removed from a valence band state or the impurity level to the conduction band. The energy cost of this process is depicted in Fig. 1 by E_{abs}.

(ii) in the second stage, if the electron was excited from the valence band, the hole left behind in the valence band lowers its energy by relaxing into the defect level. At this point the system is in the excited configuration, denoted by $E[V^nD^{m-1}C^1]$ (upper parabola), corresponding to the electron in the conduction band bound to the positively charged, $m-1$ electron defect ("impurity bound exciton").

(iii) after the vertical electronic transition into this excited state the system relaxes via phonon emission. The Frank-Condon shift in energy associated with this process in the charged ($m-1$ electrons) defect is denoted in Fig. 1 by E_{FC}^{m-1}.

(iv) in the relaxed excited state the system has a finite probability to make a radiative transition to the ground state, which results in the PL emission with energy E_{PL}.

(v) since the electronic transition is much faster than the ionic response to it, the true ground state is reached only after phonon emission (E_{FC}^m). The transition energy associated with the luminescence process with *no* phonon emission is called the zero phonon line (E_{ZPL}).

The energy E_{ZPL} of the zero phonon line can be thought of as an electronic transition where the ionic configuration can follow the electronic transition adiabatically. Therefore, E_{ZPL} can be determined as (Fig. 1)

$$E_{\text{ZPL}} = E[V^nD^{m-1}C^1] - E[V^nD^mC^0], \tag{1}$$

where the total energies correspond to equilibrium configurations i.e. minima of the two parabola in Fig. 1. We further define the exciton binding energy as [6]

$$E_b = E_{\text{gap}} - E_{\text{ZPL}}, \tag{2}$$

where E_{gap} denotes the band gap energy. We will use Eqs. (1) and (2) to calculate the binding energy of the impurity-bound exciton.

The Franck-Condon energy E_{FC}^m can be calculated as

$$E_{FC}^m = E_{\text{ZPL}} - E_{\text{PL}}. \tag{3}$$

If we define $E_{q'}^q$ to be the total energy of the defect system in charge state q with atomic configuration fixed at the fully relaxed structure for charge state q', using this notation we can express the Franck-Condon shifts alternatively as $E_{FC}^m = E_+^0 - E_0^0$ and $E_{FC}^{m-1} = E_0^+ - E_+^+$.

III. METHOD OF CALCULATION

A. LDA total energies

Our self-consistent plane-wave pseudopotential method is based on DFT applying LDA for the exchange-correlation term as parametrized by Perdew and Zunger [23]. In order to treat efficiently the localized nitrogen $2p$ orbitals using a plane-wave basis, an ultra-soft pseudopotential is used for nitrogen [24]. For Ga, As, and P we use standard norm-conserving pseudopotentials [25] with the non-linear core-valence exchange-correlation scheme [26] and treat s as the local component. With this choice of pseudopotentials, the applied 25 Ry kinetic-energy cut-off guarantees an excellent convergence with respect to the plane-wave basis. The electronic structure optimization is done using damped second-order dynamics [27] combined with the Williams-Soler [28] algorithm. All the calculations based on LDA method have been performed with a supercell containing 64 atomic sites in the zinc-blende structure. To ensure an adequate Brillouin-zone sampling we use a $2 \times 2 \times 2$ k-point mesh [29] (four k-points in the case of no assumptions of symmetry). The atomic relaxation was performed assuming no symmetry constraints, and the initial atomic positions were randomized with a maximum cartesian amplitude of 0.25 a.u. in order to break metastable symmetries which may prevent the system from reaching the true ground-state geometry. Several aspects in the LDA method need special attention in order to obtain the E_{ZPL} and E_b and are addressed below.

B. Avoiding the LDA band gap error in calculating the exciton binding energy

The band gaps in LDA calculations are typically underestimated [30]. Thus, occupation of the lowest LDA conduction band in calculating the total energy of the excited state $E[V^n D^{m-1} C^1]$ [Eq. (1)] can lead to errors. We circumvent this problem by transferring the electron removed from the defect level to a uniform jellium background whose energy is the *measured* gap, rather than to the LDA conduction band (C^1) (in fact, the supercell has to be neutral in order to avoid spurious interactions between the periodic images). Due to the expected extended character of the electron wavefunction in the conduction band bound to the hole at the impurity site, we believe that this approximation has little effect on the actual atomic geometry in the excited configuration. Using the total energy values of the fully relaxed configurations we can calculate the zero phonon line as

$$E_{\rm ZPL} = \{\epsilon_{\rm gap} + E[V^n D^{m-1} J^1]\} - E[V^n D^m J^0], \quad (4)$$

where we use the *experimental* band gap value for $\epsilon_{\rm gap}$ to avoid the LDA error, and J^1 denotes an electron in jellium. Using the definition for the exciton binding energy in Eq. (2) we find

$$E_b = E[V^n D^m J^0] - E[V^n D^{m-1} J^1]. \quad (5)$$

Our next step is to build the connection between the thermal ionization levels and E_b. We write the total energy of defect in charge state q with respect to the total energy of the neutral defect as [31]

$$E^q_{tot} = E[V^n D^{m-q} J^q] - E[V^n D^m J^0] + q(\epsilon_v + \epsilon_F), \quad (6)$$

where we have adopted the common practice to measure the electron Fermi energy ϵ_F with respect to the valence band maximum ϵ_v. The ionization levels $\epsilon(q,q')$ are defined as the values of ϵ_F when the total energies of two charge states become equal. In particular, writing the total energies [using Eq. (6)] for the neutral and singly positive charge states, the $(+/0)$ ionization level is given by

$$\epsilon(+/0) = E[V^n D^m J^0] - E[V^n D^{m-1} J^1]. \quad (7)$$

Thus, comparing Eqs. (5) and (7) we can identify E_b as the position of the single-donor $\epsilon(+/0)$ ionization level measured with respect to valence band maximum ϵ_v.

C. Determination of the energy of the valence band maximum in an impurity-containing supercell

In calculations with finite and small supercell size one needs to know how to calculate ϵ_v, the energy of an electron at the valence band maximum (VBM). A widely applied practice in defect calculations is to assign ϵ_v to the single-particle VBM eigenvalue (at Γ in GaN). However, the calculated eigenvalue in the small defect-containing supercell $\epsilon_{{\rm VBM},D}(\Gamma)$ may deviate considerably from the anticipated value in the defect-containing infinite solid, since the defect can induce a significant distortion to the band-structure. Therefore, we estimate $\epsilon_{{\rm VBM},D}(\Gamma)$ based on the eigenvalue $\epsilon_{{\rm VBM},H}(\Gamma)$ obtained from of pure bulk host (H) crystal, corrected by the difference in the average potential $\overline{V}_D$ in a bulk-like region of the defect-containing supercell and the same average potential in the defect-free supercell $\overline{V}_H$ [32–34]

$$\epsilon_v = \epsilon_{{\rm VBM},D}(\Gamma) = \epsilon_{{\rm VBM},H}(\Gamma) + (\overline{V}_D - \overline{V}_H). \quad (8)$$

This procedure is illustrated in Fig. 2. The average potential is defined as the average of the screened local potential ($V_H + V_{xc} + V^{loc}_{ps}$). The small non-local component of V_{ps} is excluded from our estimate. In the case of our 64 atom supercell the best choice for the averaging region was found to be the one of the four tetrahedral interstitial sites farthest from the defect. Each $\overline{V}$ was calculated by averaging over a $3 \times 3 \times 3$ grid (27 points in the Fourier grid of total size $54 \times 54 \times 54$). The interstitial region was found to be an optimal choice for the averaging since the effective potential behaves smoothly in this region and therefore small differences in the atomic positions between the relaxed and ideal bulk supercell have a negligible effect on the average value, in contrast to averaging at an atomic site with fast varying effective potential. The same effective potential alignment is also applied for all the presented single-partice eigenvalues below. The magnitude of the alignment $\overline{V}_D - \overline{V}_H$ for each defect is shown in Table I.

D. Correcting the error of replacing a total energy difference by an LDA eigenvalue

A question that still remains to be addressed for ϵ_v is whether the single-particle eigenvalue $\epsilon_{{\rm VBM},D}(\Gamma)$ of Eq. (8) gives a good estimate for the *total* energy change corresponding to transferring an electron from VBM to the reservoir formed by the uniform background charge (jellium). For this purpose, we can define ϵ_v alternatively as

$$\epsilon_v(N \to \infty) = E_{bulk}[V^n J^0] - E_{bulk}[V^{n-1} J^1], \quad (9)$$

which becomes an exact formulation for ϵ_v at the limit of an infinitely large supercell, where the effect of the neutralizing background charge vanishes. We define the error made by replacing the total energy difference by an eigenvalue as

$$\delta_{\mathbf{k}} = E_{bulk}[V^n J^0] - E_{bulk}[V^{n-1} J^1] - \epsilon_{{\rm VBM},H}(\mathbf{k}). \quad (10)$$

Here $\mathbf{k}$ corresponds to the k-point used for Brillouin zone integration [in the case of 64 atom zinc-blende bulk supercell the 2x2x2 Monkhorst-Pack grid reduces to a single special k-point $(\frac{1}{4},\frac{1}{4},\frac{1}{4})$]. In our case of 64 atom GaN supercell, we find $\delta_{\mathbf{k}} = -0.018$ eV. We use this value obtained at the special k-point as an estimate for the $\delta_{\mathbf{k}}$ at Γ in the defect supercell. This value is relatively small suggesting only minor effect for ϵ_v in GaN. However, recent calculations in $CuInSe_2$ [35] suggest that $\delta_{\mathbf{k}}$ may experience much larger values in other materials.

Thus, combining the Eqs. (8), (9) and (10), the valence band maximum energy becomes

$$\epsilon_v = \epsilon_{\mathrm{VBM},H}(\Gamma) + (\overline{V}_D - \overline{V}_H) + \delta_{\mathbf{k}}, \tag{11}$$

which concludes our analysis of estimating ϵ_v in finite-size supercells.

IV. ELECTRONIC AND ATOMIC STRUCTURE OF GA$\underline{\text{N}}$:P AND GA$\underline{\text{N}}$:AS

A. Atomic geometries

We discuss impurity-induced atomic relaxation by considering the ratio

$$d^{(i)} \equiv R^{(i)}_{\mathrm{Ga-X}}/R^{0}_{\mathrm{Ga-N}}, \tag{12}$$

where $R^{(i)}_{\mathrm{Ga-X}}$ denotes i-th bond length ($i = 1,2,3,4$) between the impurity X and the nearest-neighbor Ga-atoms in the Ga$\underline{\text{N}}$:X system, and $R^{0}_{\mathrm{Ga-N}}$ is the corresponding quantity in the pure GaN host, where all four bonds are equivalent. A positive ratio $d^{(i)}$ implies outward relaxation. Symmetry-conserving relaxation means that the $d^{(i)}$ are equal for all i. Results for neutral defects are shown in Table II. For comparison, the values based on the valence force-field method (VFF) applied in Ref. [2] are also given.

Based on the larger covalent radii for P and As than for N, an outward relaxation of the four neighboring Ga is expected. The values in Table II indeed confirm this expectation. We find a $\sim 13\%$ relaxation for Ga$\underline{\text{N}}$:P and $\sim 15\%$ for Ga$\underline{\text{N}}$:As, respectively. The relaxation in the neutral charge state with complete shell t^6 is found to conserve the tetrahedral symmetry. It is slightly larger for As than for P, consistent with the larger atomic size. The values obtained with the LDA and VFF methods are in good agreement with each other. To estimate the convergence in relaxation with respect to supercell size, we have also performed the VFF calculations with both 64 and 512 atoms supercells. The minor differences found between 64 and 512 atom cells verifies that a 64 atom supercell is realistic for the study of *isolated* point defects.

We also give in Table II the ratio $R^{(i)}_{\mathrm{Ga-X}}/R^{0}_{\mathrm{Ga-X}}$ normalized to the bond length $R^{0}_{\mathrm{Ga-X}}$ in the "complementary solid". This shows to what extent the relaxation of the Ga$\underline{\text{N}}$:X system produces bond lengths that are similar to the pure GaX host crystal. We see that the local structure around the impurity leads to bond lengths that are slightly *shorter* than the *ideal* Ga-X bond length. This was predicted by Martins and Zunger [36]. For P (As) impurities this ratio reveals about seven (eight) percent shorter bonds than in the GaX bulk.

The geometry of *charged* Ga$\underline{\text{N}}$:P^+ and Ga$\underline{\text{N}}$:As^+ is an interesting subject, since the electronic configuration is isoelectronic with V^-_{Zn} in ZnSe. The experimental results by Watkins [40] have shown that V^-_{Zn} in ZnSe undergoes a significant Jahn-Teller symmetry lowering atomic distortion [41] induced by the localization of the hole wavefunction on one of the nearest Se neighbors. The model proposed by Watkins [40] suggests that this is due to breakdown of the triply degenerate t_2^6 level into e^4 and a_1^1 levels. The associated Jahn-Teller relaxation energy is estimated to be 0.35 eV [40]. Surprisingly, LDA calculations for V^-_{Zn} in ZnSe [37] fail to reproduce the experimentally observed large Jahn-Teller relaxation.

We have thus searched for a Jahn-Teller distortion in Ga$\underline{\text{N}}$:P^+ and Ga$\underline{\text{N}}$:As^+. First, we created a starting geometry corresponding to the zinc-blende structure with slight (maximum cartesian amplitude 0.25 a.u.) random displacements of all atoms. This was done in order to break possible metastable symmetric configurations. Then we let all atoms move according to the calculated quantum mechanical forces (without any symmetry constraints) until the total energy minimum was reached. The resulting bond lengths are shown in Table III. We observe roughly one percent increase in the outward relaxation of the neighboring Ga atoms compared with the neutral charge state. Furthermore, a slight symmetry lowering relaxation (i-dependent $d^{(i)}$) is detected, which, however, cannot be decomposed into Jahn-Teller distortion exhibiting C_{3v} symmetry. We then made tests with other starting geometries, where the impurity atom was displaced along the positive or negative [111] direction by various amounts up to half the ideal nearest neighbor distance. No randomization of the atomic positions was performed. After full atomic relaxation the system did not maintain the C_{3v} symmetry, but the results revealed structures similar to presented in Table III. These configurations were energetically degenerate (within 1 meV from the configuration in Table III), but exhibited slightly differing bond lengths from values in Table III with deviation amplitude of about 0.5 percent. We also studied the Jahn-Teller geometry for V^-_{Zn} in ZnSe proposed by Watkins [40] by moving As or P impurity along the positive or negative [111] directions (keeping all other atoms at their ideal positions). However, in both directions the total energy as well as the defect orbital energies of the split levels moved *up* upon displacement from the tetrahedral geometry. We thus conclude that for Ga$\underline{\text{N}}$:P^+

and Ga$\underline{\text{N}}$:As$^+$ LDA gives no Jahn-Teller distortion with C_{3v} symmetry.

For the doubly positive charge states the outward relaxation the the neighboring Ga atoms further increases by $\sim 1\%$ (Table III). All bonds have unequal length i.e. similar to the singly positive charge state the configuration lacks any clear symmetry.

B. Defect energy levels and wavefunctions

Accompanied by the large outward relaxation of the Ga atoms surrounding the P and As impurities we detect the appearance of a *deep* impurity level in the band gap. The positions of the single-particle levels are shown in Fig. 3. The results reveal that the neutral impurity-induced deep level is three-fold degenerate consisting of p-like orbitals. Figure 4 shows the electronic density (wavefunction squared) of the three-fold degenerate level for the neutral Ga$\underline{\text{N}}$:As. The wavefunction can be seen to be primarily localized on the impurity site, with a minor contribution near the next-nearest neigbor nitrogen atoms. The LDA single-particle levels for the neutral charge state are in qualitative agreement with the ones given by EPM [2–4]: the position of the P (As) derived level in the neutral charge state in the LDA calculations is $\epsilon_v + 0.40$ ($\epsilon_v + 0.60$) eV while the EPM results are slightly higher at $\epsilon_v + 0.61$ ($\epsilon_v + 0.75$) eV. We note that the band gap found in the LDA calculations was 2.67 eV [30] while in the empirical pseudopotential method the pseudopotentials were fitted to reproduce the experimental band gap (3.3 eV). To see the effect that the different band gaps can have on the position of the defect level we analysed the character of the deep impurity states by projection to valence and conduction band states of the pure host material [39]. The results showed that the deep states possessed very dominantly a valence band character with very little overlap with the conduction band states. This suggests that the positions (with respect to ϵ_v) of the single-particle levels found in our LDA calculations are little affected by the actual underestimate in the band gap value, and thus this band gap underestimation is not the principal factor in the difference between LDA and EPM results.

Turning to the charged defects, we find a minor splitting (a few meV) in the three-fold degenerate level in the singly positive charge state, where an electron is removed from the defect level [Fig. 3]. Furthermore, the single particle levels move closer to the valence band edge as the occupancy of the level is reduced, reflecting a diminished interelectronic Coulomb repulsion.

C. Transition energies: theory and experiment

Figure 5 illustrates the total energies of Ga$\underline{\text{N}}$:P and Ga$\underline{\text{N}}$:As defects in various charge states as a function of the Fermi-level position [Eq. (6)]. The ionization levels, i.e. the Fermi-level values where the total energies of two charge states become equal [e.g., Eq. (7)], are shown as solid dots. For both defects we find the neutral, and singly and doubly positive charge states. The donor levels are found at

$$\begin{aligned}\epsilon(+/0) &= \epsilon_v + 0.22 \;\; (\text{Ga}\underline{\text{N}}:\text{P}) \\ \epsilon(+/0) &= \epsilon_v + 0.41 \;\; (\text{Ga}\underline{\text{N}}:\text{As})\end{aligned} \tag{13}$$

$$\begin{aligned}\epsilon(++/+) &= \epsilon_v + 0.09 \;\; (\text{Ga}\underline{\text{N}}:\text{P}) \\ \epsilon(++/+) &= \epsilon_v + 0.24 \;\; (\text{Ga}\underline{\text{N}}:\text{As})\end{aligned}$$

The recent photoluminescence experiments for P-implanted GaN by Jadwisienczak and Lozykowski [19] give the PL line at $E_{\mathrm{PL}} = 2.917$ eV, in good agreement with the results by Pankove and Hutchby [17] and Metcalfe *et al.* [18]. Jadwisienczak and Lozykowski [19] have further determined the zero phonon line to be at $E_{\mathrm{ZPL}} = 3.2709$ eV. The exciton binding energy according to Eq. (2) is thus $E_b = E_{\mathrm{gap}} - E_{\mathrm{ZPL}} = 0.232$ eV, assuming $E_{\mathrm{gap}} = 3.503$ eV as the band gap in their wurtzite samples. According to Eqs. (5) and (7) we can identify the (+/0) ionization energy in our calculations as E_b. Therefore our result $E_b = 0.22$ eV [Eq. (13)] is in excellent agreement with the experimental value.

The calculated values for the Franck-Condon shifts are shown in Table IV. Comparison of E^m_{FC} in the case of Ga$\underline{\text{N}}$:P to the experimental shift between the PL and ZPL (0.35 eV) shows that the calculated values are considerably smaller. On the other hand, the small Franck-Condon shifts are consistent with the relatively small atomic relaxation differences between the neutral and positive charge states described in Table III.

V. CONCLUSIONS

The self-consistent plane-wave pseudopotential calculations verify the exceptional behavior of isovalent P and As impurities in GaN: both substitutional impurities are found to induce deep levels in the band gap in contrast with all other conventional III-V systems. The defect levels are triply degenerate t_2-like orbitals primarily localized at the substitutional atom. The calculated total energies are used to estimate zero phonon line and impurity bound exciton binding energies associated with the photoluminescence measurements. The calculated exciton binding energy $E_b = 0.22$ eV for Ga$\underline{\text{N}}$:P is in excellent agreement with the available experimental data $E_b = 0.232$ eV.

ACKNOWLEDGMENTS

We thank S. B. Zhang and L. Bellaiche for many helpful discussions. T. M. gratefully acknowledges the financial support provided by the Väisälä Foundation (Helsinki, Finland). This work is supported in part by the U.S. Department of Energy, OER-BES-DMS, Grant No. DE-AC36-83-CH10093.

---

[1] Electronic address: tmattila@nrel.gov
[2] Electronic address: alex_zunger@nrel.gov

[1] Landolt-Börnstein, *Numerical Data and Functional Relationships in Science and Technology*, (Springer,Berlin,1982).
[2] L. Bellaiche, S.-H. Wei, and A. Zunger, Phys. Rev. B **54**, 17568 (1996).
[3] L. Bellaiche, S.-H. Wei, and A. Zunger, Appl. Phys. Lett. **70**, 3558 (1997).
[4] L. Bellaiche, S.-H. Wei, and A. Zunger, Phys. Rev. B. **56**, 10233 (1997).
[5] J.D. Cuthberg and D. G. Thomas, J. Appl. Phys. **39**, 1573 (1968).
[6] D. M. Roessler, J. Appl. Phys. **41**, 4589 (1970).
[7] D. Hennig, O. Goede, and W. Heimbrodt, Phys. Status Solidi B **113**, K163 (1982).
[8] O. Goede and W. Heimbrocht, Phys. Status Solidi B **110**, 175 (1982).
[9] O. F. Vyvenko, I. A. Davydov, V. G. Luchina, and S. L. Tselishchev, Fiz. Tekh. Poluprovodn. **25**, 1745 (1991). [Sov. Phys. Semicond. **25**, 1050 (1991).]
[10] G. W. Iseler and A. J. Strauss, J. Lumin. **3**, 1 (1970).
[11] T. Fukushima and S. Shionoya, Jpn. J. Appl. Phys. **12**, 549 (1973).
[12] M. Kondow, K. Uomi, K. Hosomi, and T. Mozume, Jpn. J. Appl. Phys. **33**, L1056 (1992).
[13] M. Weyers, M. Sato, and H. Ando, Jpn. J. Appl. Phys. **31**, L853 (1992).
[14] A. Rubio and M. L. Cohen, Phys. Rev. B **51**, 4343 (1995).
[15] J. Neugebauer and C. G. Van de Walle, Phys. Rev. B **51**, 10568 (1995).
[16] S.-H. Wei and A. Zunger, Phys. Rev. Lett. **76**, 664 (1996).
[17] J. I. Pankove and J. A. Hutchby, J. Appl. Phys. **47**, 5387 (1976).
[18] R. D. Metcalfe, D. Wickenden, and W. C. Clark, J. Lumin. bf 16, 405 (1978).
[19] W. M. Jadwisienczak and H. J. Lozykowski, 'Photoluminescence from GaN Implanted with Isoelectronic Phosphorus and Bismuth', Proceedings of the 24th International Symposium on Compound Semiconductors, San Diego, USA, 1997.
[20] For a review of plane-wave pseudopotential methods based on DFT and LDA, see M. C. Payne, M. P. Teter, and D. C. Allan, T. A. Arias, and J. D. Joannopoulos, Rev. Mod. Phys. **64**, 1045 (1992).
[21] P. Hohenberg and W. Kohn, Phys. Rev. **136**, B864 (1964).
[22] D. M. Ceperley and B. J. Alder, Phys. Rev. Lett. **45**, 566 (1980).
[23] J. Perdew and A. Zunger, Phys. Rev. B **23**, 5048 (1981).
[24] D. Vanderbilt, Phys. Rev. B **41**, 7892 (1990); K. Laasonen *et al.*, Phys. Rev. B **47**, 10142 (1993).
[25] G. B. Bachelet, D. R. Hamann, and M. Schüter, Phys. Rev. B **26**, 4199 (1982). D. R. Hamann, Phys. Rev. B **40**, 2980 (1989). Our pseudopotentials are verified to be ghost-free using the method by X. Gonze, R. Stumpf and M. Scheffler, Phys. Rev. B **44**, 8503 (1991).
[26] S. G. Louie, S. Froyen, and M. L. Cohen, Phys. Rev. B **26**, 1738 (1982).
[27] F. Tassone, F. Mauri and R. Car, Phys. Rev. B **50**, 10561 (1994).
[28] A. Williams and J. Soler, Bull. Am. Phys. Soc. **32**, 409 (1952).
[29] H. J. Monkhorst and J. D. Pack, Phys. Rev. B **13**, 5188 (1976).
[30] See e.g. Ref [23]. The band gap obtained for c-GaN in our calculations is 2.67 eV while the experimental value is 3.3 eV [42]. The band gap is calculated at the theoretical lattice constant (4.39 Å) which is about 3 percent smaller than the experimental value. This underestimation is due to the overbinding of LDA and the absence of a Ga $3d$-orbital in the method applied.
[31] S. B. Zhang and J. E. Northrup, Phys. Rev. Lett. **67**, 2339 (1991).
[32] D. B. Laks, C. G. Van de Walle, G. F Neumark, P. E. Blöchl and S. T. Pantelides, Phys. Rev. B **45**, 10965 (1992).
[33] A. Garcia and J. E. Northrup, Phys. Rev. Lett. **74**, 1131 (1995).
[34] S. Pöykkö, M. J. Puska, and R. M. Nieminen, Phys. Rev. B **53**, 3813 (1996).
[35] S. B Zhang, S.-H. Wei, and A. Zunger, InCuSe submitted.
[36] J. L. Martins and A. Zunger, Phys. Rev. B **30**, 6217 (1984).
[37] S. Pöykkö *et al*, "Nitrogen-impurity–native-defect complexes in ZnSe", submitted to Phys. Rev. B.
[38] T. Mattila, S. Pöykkö, and R. M. Nieminen, Phys. Rev. B (Dec 15, 1997).
[39] P. Boguslawski, E. L. Briggs, and J. Bernholc, Phys. Rev. B **51**, 17255 (1995).
[40] G. D. Watkins, in *Defect Control in Semiconductors, Proceedings of the International Conference on the Science and Technology of Defect Control in Semiconductors*, Yokohama, 1989, edited by K. Sumino (North-Holland, Amsterdam, 1990), p. 933.
[41] We consider here the static (i.e. not dynamic) Jahn-Teller effect where the system is able to lower its total energy by a symmetry lowering atomic relaxation associated with the removal of electronic orbital degeneracy.
[42] S. Strite, M. E. Lin, and H. Morkoç, Thin Solid Films **231**, 197 (1993).

TABLE I. The magnitudes of effective potential alignment [see Eq. (8)] for the studied defects.

Defect	$\overline{V}_D - \overline{V}_H$
P_N^0	0.09
P_N^+	0.14
P_N^{++}	0.19
As_N^0	0.11
As_N^+	0.17
As_N^{++}	0.22

TABLE II. The ratio $R^{(i)}_{\mathrm{Ga-X}}$ / $R^0_{\mathrm{Ga-N}}$ [Eq.(12)] between the Ga-to-impurity (X=P,As) nearest neighbor bond length and the Ga-N bond length in pure bulk GaN. The ratio $R^{(i)}_{\mathrm{Ga-X}}$ / $R^0_{\mathrm{Ga-X}}$ is also given to allow comparison with the bond length in bulk GaX. The results correspond to *neutral* defects as calculated by the self-consistent plane-wave pseudopotential method (LDA) and by the valence force-field method (VFF). In all cases tetrahedral symmetry is found to be conserved i.e. the four nearest neighbor bonds are equivalent. Theoretical values for $R^0_{\mathrm{Ga-N}}$ are used: in the VFF method the bulk bond length is identical with the experimental value, but in the LDA calculations the bond length deviates from the experimental value due to overbinding in LDA [30]. The numbers in the parenthesis refer to the supercell size.

	LDA (64)		VFF (64)		VFF (512)	
	$R_{\mathrm{Ga-X}}$ / $R^0_{\mathrm{Ga-N}}$	$R_{\mathrm{Ga-X}}$ / $R^0_{\mathrm{Ga-X}}$	$R_{\mathrm{Ga-X}}$ / $R^0_{\mathrm{Ga-N}}$	$R_{\mathrm{Ga-X}}$ / $R^0_{\mathrm{Ga-X}}$	$R_{\mathrm{Ga-X}}$ / $R^0_{\mathrm{Ga-N}}$	$R_{\mathrm{Ga-X}}$ / $R^0_{\mathrm{Ga-X}}$
Ga$\underline{\mathrm{N}}$: P	1.132	0.930	1.127	0.932	1.131	0.936
Ga$\underline{\mathrm{N}}$: As	1.155	0.914	1.145	0.913	1.151	0.918

TABLE III. The ratio $d^{(i)} = R^{(i)}_{\mathrm{Ga-X}}$ / $R^0_{\mathrm{Ga-N}}$ [Eq. (12)] between the Ga-X (X=P,As) and the Ga-N bond length in bulk GaN for the *singly* and *doubly positive* charge states as calculated by the self-consistent plane-wave pseudopotential method (LDA).

Defect	$d^{(1)}$	$d^{(2)}$	$d^{(3)}$	$d^{(4)}$
Ga$\underline{\mathrm{N}}$: P^0	1.132	1.132	1.132	1.132
Ga$\underline{\mathrm{N}}$: P^+	1.147	1.150	1.146	1.144
Ga$\underline{\mathrm{N}}$: P^{++}	1.159	1.165	1.157	1.152
Ga$\underline{\mathrm{N}}$: As^0	1.155	1.155	1.155	1.155
Ga$\underline{\mathrm{N}}$: As^+	1.171	1.178	1.173	1.168
Ga$\underline{\mathrm{N}}$: As^{++}	1.185	1.200	1.187	1.179

TABLE IV. The calculated Franck-Condon shifts for P and As impurities in GaN given by the LDA method.

Defect	E^{m}_{FC} (eV)	E^{m-1}_{FC} (eV)
P_N	0.08	0.06
As_N	0.11	0.09

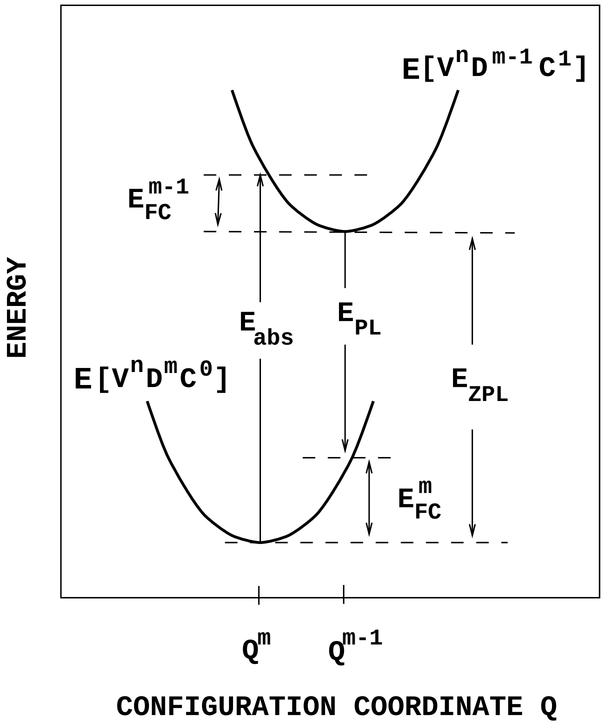

FIG. 1. Schematic configuration coordinate diagram of the luminescence transitions associated with the isovalent impurities in GaN.

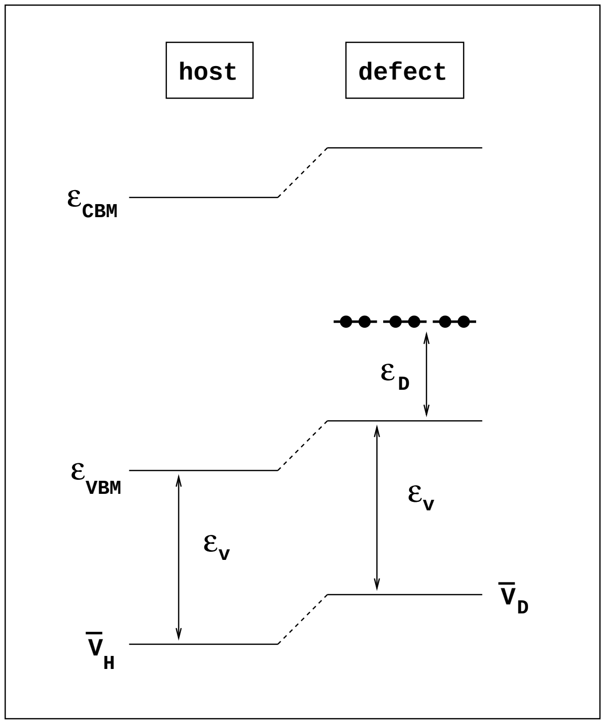

FIG. 2. Schematic illustration of the average effective potential alignment of the single-particle levels between bulk and defect supercells. $\overline{V}_D$ denotes the average effective potential in the bulk-like region in the defect supercell and $\overline{V}_H$ denotes the same quantity calculated in the same region in the bulk supercell of the same size.

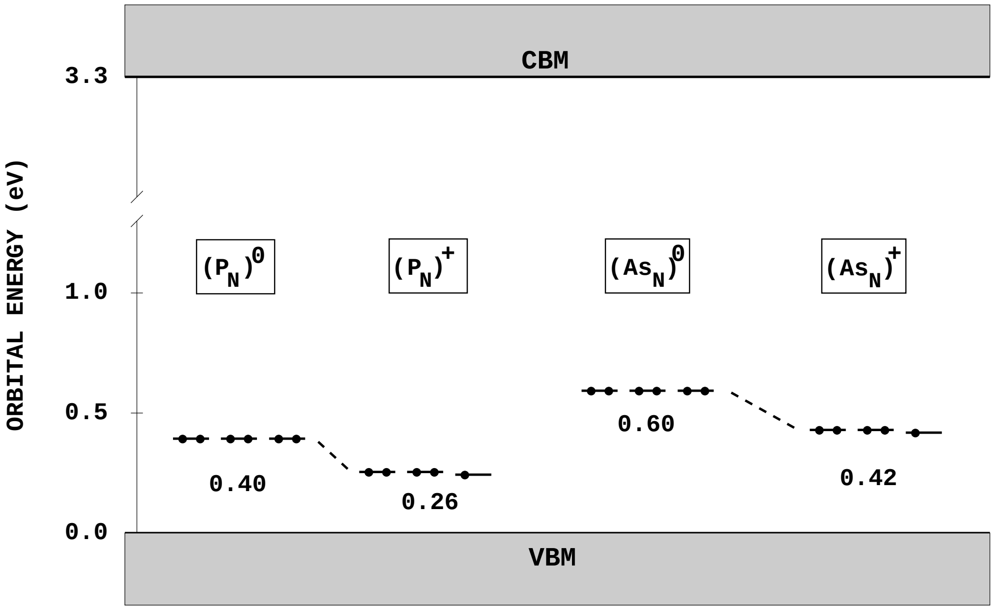

FIG. 3. The single-particle levels for P and As impurities in GaN in the neutral and singly positive charge states as obtained in the LDA calculations. The positions of the single-particle levels are given with respect to the valence band maximum ϵ_v derived for each case according to the alignment based on the average effective potential described in Eq. 8.

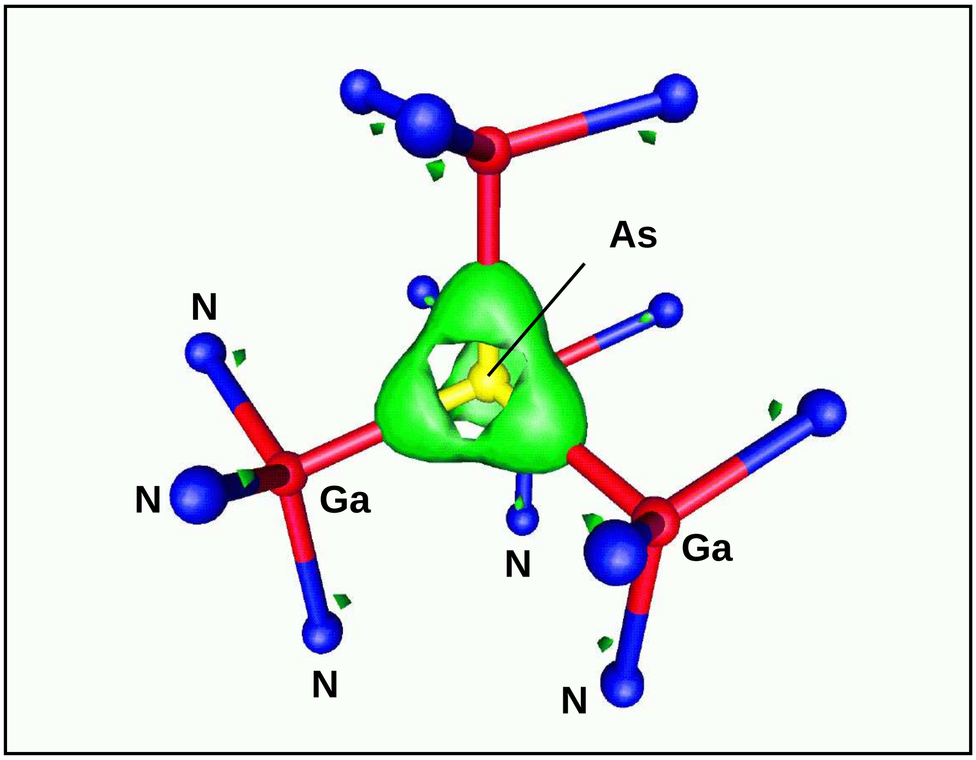

FIG. 4. The wavefunction squared associated with the deep As-impurity induced level in GaN. The densities of the three degenerate levels are added together before drawing the isosurface at the density 0.025 e/Bohr^3.

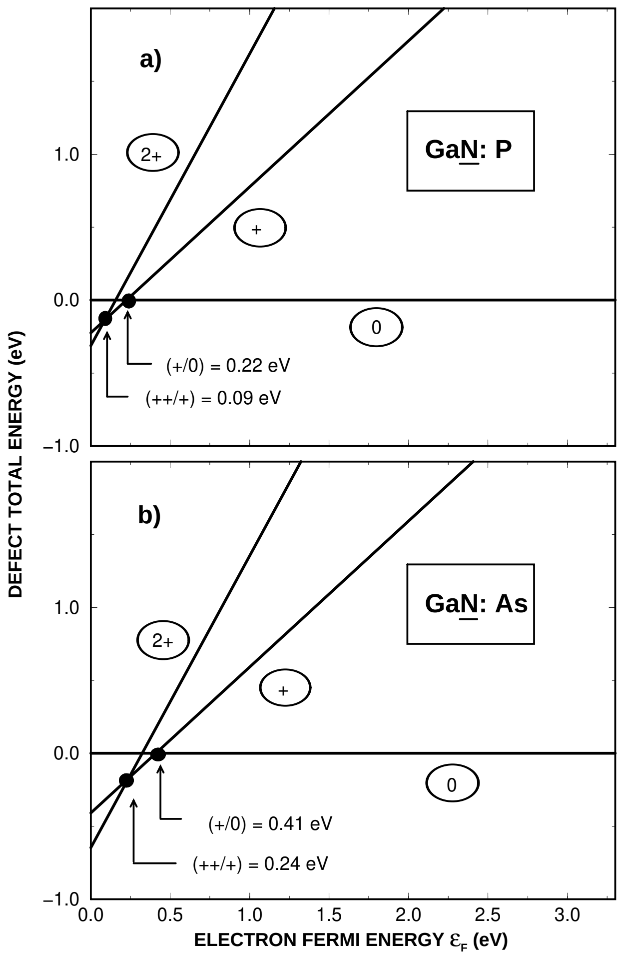

FIG. 5. Total energies of a) Ga$\underline{\mathrm{N}}$:P and b) Ga$\underline{\mathrm{N}}$:As defect in 0,+, and ++ charge states as a function of the electron Fermi energy. The ionization levels are depicted with solid dots.